Multifractal analysis of crack patterns in reinforced concrete shear walls

A. Ebrahimkhanlou[1], A. Farhidzadeh[2], S. Salamone[3*]

Abstract

Conventionally, the assessment of reinforced concrete shear walls (RCSW) relies on manual visual assessment which is time-consuming and depends heavily on the skills of the inspectors. The development of automated assessment employing flying and crawling robots equipped with high resolution cameras and wireless communications to acquire digital images and advance image processing to extract cracks pattern, has paved the path toward

[1] Ph.D. Candidate, *Smart Structures Research Laboratory (SSRL), Department of Civil Architectural and Environmental Engineering , University of Texas at Austin, 10100 Burnet Rd, Bldg 177, Austin, TX 78758* Email: *arvinebr@utexas.edu;* Lab: *+1 (512) 471-3024*

[2] Ultrasonics Research Scientist, *Mistras Group Inc., Products & Systems division Department,* Email: *alireza.farhidzadeh@gmail.com*

[3]* Assistant Professor, Director *Smart Structures Research Laboratory (SSRL), Department of Civil Architectural and Environmental Engineering , University of Texas at Austin, 301 E Dean Keeton, C1748, Room ECJ 4.710, Austin, TX 78712;* Email*:* : salamone@utexas.edu*;* Tel: +1 (512) 232-3427; corresponding author

implementing an automated system which determines structural damage based on visual signals acquired from structures. Since there are few if any studies to correlate crack patterns to structural integrity this paper proposes to analyze crack patters by using a Multifractal Analysis (MFA). The approach is initially tested on synthetic crack patterns, then it is applied to a set of experimental data collected during the testing of two large-scale RCSW subjected to controlled reversed cyclic loading. The structural response data available for each specimen is used to link the multifractal parameters with the structural performance of the two specimens. A relationship between the multifractal parameters and the cracks patterns evolution and mechanism is noted. The results show that as the cracks patterns extend and grow, multifractal parameters move toward higher values. The parameters jump as the mechanical response show severe stiffness loss. In this study no attempt is made to automate the process of mapping cracks from images.

Keywords

Multifractal Analysis, Visual Assessment, Damage Assessment, Surface Crack Patterns, Reinforced Concrete Structures

Introduction

Reinforced concrete shear walls (RCSW) are one of the most commonly used seismic resisting systems in conventional buildings and infrastructures. RCSWs are subjected to deterioration due to aging, increased load, and natural hazards. To secure the overall soundness of these structures proper assessment is crucial. Commonly, RCSWs are assessed visually by tracking defects such as corrosion and spalling, and quantifying the length and the width of existing cracks[1,2]. Concrete bridge decks are also commonly assessed based on cracks density[3,4]. Worldwide, various condition-rating grades have been developed to quantify damage conditions in terms of crack's width and length [5–7]. Although manual visual inspection (VI) is a well-established method to inspect RCSWs, it is time-consuming and depends heavily on the skills of the inspectors. Moreover, it may take weeks to obtain access to buildings hit by natural hazards, such as earthquake. In order to overcome these limitations, automated-based VI is a field that has received significant interest over the past few years. Automatic inspection techniques use flying and crawling robots equipped with high resolution camera and wireless communications to acquire 2D digital images; then image processing is used to automatically retrieve damage properties, such as crack length and width [8–10], [11,12]. Despite their increasing usage in the last few years few automated visual inspection methods if any other than the authors recent publication exists[13] to link the effect

of damage to the overall soundness of the structure. Current systems simply relay the information about crack length and width to engineers that then determine the course of action: retrofit, replacement, or no action. The results presented in this paper are part of a long-term project that aims at developing an automated-based inspection technology for the nondestructive evaluation (NDE) of reinforced concrete structures. The technology is based on the fractal analysis of 2D images taken in the visible spectrum, to retrieve surface defect patterns that can provide a quantitative measure of damage. Fractal analysis is a relatively novel mathematical tool that has been used successfully in many fields including biology and physical sciences [14–17]. However, its application in the NDE/SHM community has been modest[18–21]. Recently, the authors have used a monofractal analysis to discriminate different damage grades in RCSWs [22]. They have shown that, in general the fractal dimension increases as the structural damage increases. Although these preliminary results using the monofractal analysis have been encouraging, it is important to recognize that using a single scalar, the fractal dimension (FD), may be insufficient as a summary statistic for the overall crack patterns. In this paper a more general approach is presented (i.e., multifractal analysis) based on point-wise scaling properties (i.e., local fractal dimensions) of the image. As cracks develop, their width, length, density, and fractal dimension grow (local change). Besides, as cracking mechanism changes, multifractal parameters form separate clusters which indicates

the change in mechanism (global change). So, the idea is to decomposed 2D images into many subsets characterized by different local FD, which quantify the local singular behavior and as a result relate to the local scaling of the image [23]. Thus, a 2D image will require a set of FD to fully characterize its scaling properties. This paper is organized as follows. First, a brief overview on the multifractal analysis is provided, and followed by application of the method on synthetic cracks. Then, experimental results are presented with application to the damage assessment of two large-scale reinforced concrete shear walls under lateral cyclic loading.

Multifractal analysis

Background

The term "Fractal" was first introduced by Mandelbrot [24] to indicate self-similar objects whose complex geometry cannot be characterized by an integer dimension. Since then, the term has been extensively used to study natural and experimental physical phenomena [25]. A common way to characterize fractal objects is by their fractal dimension (FD) which, very roughly speaking, is related to their degree of complexity, and the extent to which features at different scales are related. More specifically, FD is defined as a ratio comparing how detail in a pattern changes with the scale at which it is measured[26]. The most popular algorithm to calculate the FD is the box-counting, which considers the space filling properties of the object

as an indication of the object's complexity [14]. In this approach, a virtual grid of squared boxes overlaps the object, and the number of boxes of a given size (r) necessary to cover it is counted. As $r \rightarrow 0$, the total area covered by the area elements converges to the measure of FD [22]. Based on this method FD is defined as:

$$FD = \lim_{r \to 0} \frac{\log N(r)}{\log(r)} \tag{1}$$

where $N(r)$ is the total number of non-empty boxes of linear size r.

Many natural phenomena, however, have a more complex scaling relation, and their statistics cannot be described by just a single scalar (i.e., FD). For instance, consider a 2D signal such as a gray scale image. For describing an object of the image the box-counting method may not be appropriate since it gives only a relation between the non-empty boxes and the box size [27]; therefore no weighting is done to the count according to the signal levels into the boxes. Multifractal analysis has shown the potential to provide more insights into the scaling properties of these objects [28] [29]. The multifractal analysis is a generalization, in which the fractal dimension (FD), instead of being a global parameter which only gives information on the support of a given measure [30], is a local parameter (called singularity strength α) that may change from box to box, and provides more insight into the way the measure is

distributed over its support [31] [28]. In multifractal analysis the scale-invariant properties of the object can be characterized on the basis of its generalized [32] dimensions D_q, defined as:

$$D_q = \frac{1}{q-1} \lim_{r \to 0} \frac{\log \sum_{i=1}^{N(r)} P_i^q(r)}{\log(r)} \tag{2}$$

where q is a real value moment order, $P_i(r)$ is the measure (or weight) associated with the i-th box. For a binary image $P_i(r)$ can be seen as the probability of existence of black pixels in that box, that is [33]:

$$P_i(r) = \frac{N_i(r)}{\sum_{i=1}^{M(r)} N_i(r)} \tag{3}$$

where $N_i(r)$ is the number of black pixels inside the i-th box of size r, and $M(r)$ is the total number of boxes containing at least one black pixel. The most popular generalized dimensions are: the capacity dimension (D_0), the information dimension (D_1), the correlation dimension (D_2). In general, D_q is a monotone decreasing function of q. If D_q is a single-

valued function, equal to the fractal dimension (FD) defined above, the object is called monofractal [14]. Overall, the parameter q serves as a "microscope" that analyzes the object at different scales [14]. In multifractal analysis, one can also determine the number of boxes having similar local scaling, that is same α , and define $f(\alpha)$ as the fractal dimension of the set of boxes with singularities α . The curve $f(\alpha)$, also called multifractal spectrum, is a convex function whose maximum corresponds to D_0. As $q \to -\infty$, $\alpha \to \alpha_{\max}$, and as $q \to +\infty$, $\alpha \to \alpha_{\min}$. In general, when $f(\alpha)$ and D_q are smooth functions of α and q, a Legendre transformation can be used to derive $f(\alpha)$ from D_q [34,35]. However, $f(\alpha)$ can also be directly calculated, without knowing D_q, by using the method proposed by Chhabra et al. [34,35]. The first step of this approach consists of defining a family of normalized measures $\mu_i(q,r)$ defines as:

$$\mu_i(q,r) = \frac{P_i(r)^q}{\sum_{i=1}^{N(r)} P_i(r)^q} \tag{4}$$

For each box *i*, the normalized measure $\mu_i(q,r)$ depends on the order of the statistical moment, and on the box size and it takes values in the range [0,1] for any value of q. Then, the two functions $\alpha(q)$ and $f(q)$ are evaluated:

$$\alpha(q) = \lim_{r \to 0} \frac{\sum_{i=1}^{N(r)} \mu_i(q,r) \log(P_i(r))}{\log(r)} \tag{5}$$

$$f(q) = \lim_{r \to 0} \frac{\sum_{i=1}^{N(r)} \mu_i(q,r) \log(\mu_i(q,r))}{\log(r)} \tag{6}$$

For each q, values of $\alpha(q)$ and $f(q)$ are obtained from the slope of plots of $\sum_{i=1}^{N(r)} \mu_i(q,r) \log(P_i(r))$ versus $\log(r)$, and $\sum_{i=1}^{N(r)} \mu_i(q,r) \log(\mu_i(q,r))$ versus $\log(r)$ over the entire range of box size values under consideration. Finally, these two data sets of $\alpha(q)$ and $f(q)$ are plotted with respect to each other to construct the singularity spectrum (i.e. plot of α vs. $f(\alpha)$).

Synthetic data analysis

The analysis of synthetic data sets presented in this section are intended to illustrate how the multifractal parameters are calculated, and show their application for crack patterns quantification in RCSWs. As shown in Figure 1, the data sets consisted of four binary images (size 500×400 pixels), representing typical crack patterns in a shear wall (size of the wall was assumed to be $5000\text{mm} \times 4000\text{mm}$). Figure 1(a) was assumed as a base pattern (CASE 0), while the other three cases were generated by simple manipulations of CASE 0. Specifically, for CASE 1 (Figure 1(b)) minor changes were applied on CASE 0, while the overall shape was preserved. CASE 2 (Figure 1(c)), was generated by flipping one of the two cracks of the base pattern. Hence, the cracks details are exactly the same, but the general shape was changed. Finally, CASE 3 is representative of crack patterns growth.

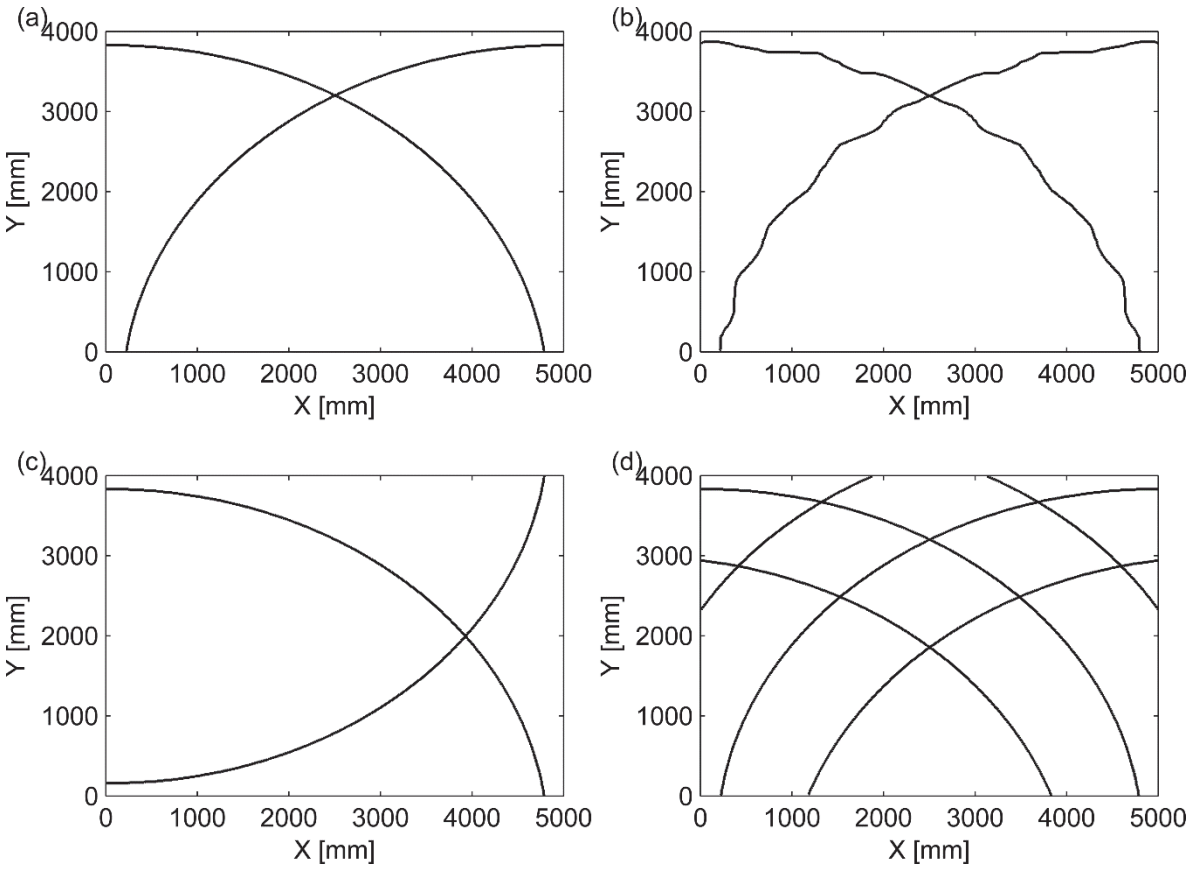

Figure 1. Synthetic crack patterns: (a) CASE 0, (b) CASE 1, (c) CASE 2, (d) CASE 3

In order to perform the multifractal analysis of these images the Chhabra method described in section 2.1 was used to directly evaluate the singularity spectrum $f(\alpha)$ and the generalized dimension D_q. The analysis was carried out by dividing each image with rectangular boxes of aspect ratio similar to the original image. The number of division ranged from 1 to 40,

(i.e., the smallest box size was equal to 12.5×10 pixels), while the range of q was selected within the range between 10 and -10 (i.e., $q \in [-10, 10]$).

Figure 2 shows $P_i(r)$ and $\mu_i(q,r)$ for the data set shown in Figure 1(a). Two different box sizes were considered, that is, 100×80 and 50×40 pixels. As expected, the higher value of $P_i(r)$ was obtained at boxes with higher concentration of black pixels. In order to illustrate the effect of the parameter q, $\mu_i(q,r)$ was calculated for three different values of q, i.e. $q \in \{-1,0,1\}$ as shown in Figure 2. It can be observed that negative values of q's ($q = -1$) are dominated by boxes of low probability densities (i.e., rare events), while positive values of q's ($q = +1$) are dominated by boxes of high probability densities (i.e., smooth events). For $q = 0$, each box is given equal weight regardless of the number of points in the boxes. Thus information concerning distribution of points in the boxes is lost. Therefore, for $q = 0$ a traditional monofractal analysis is recovered.

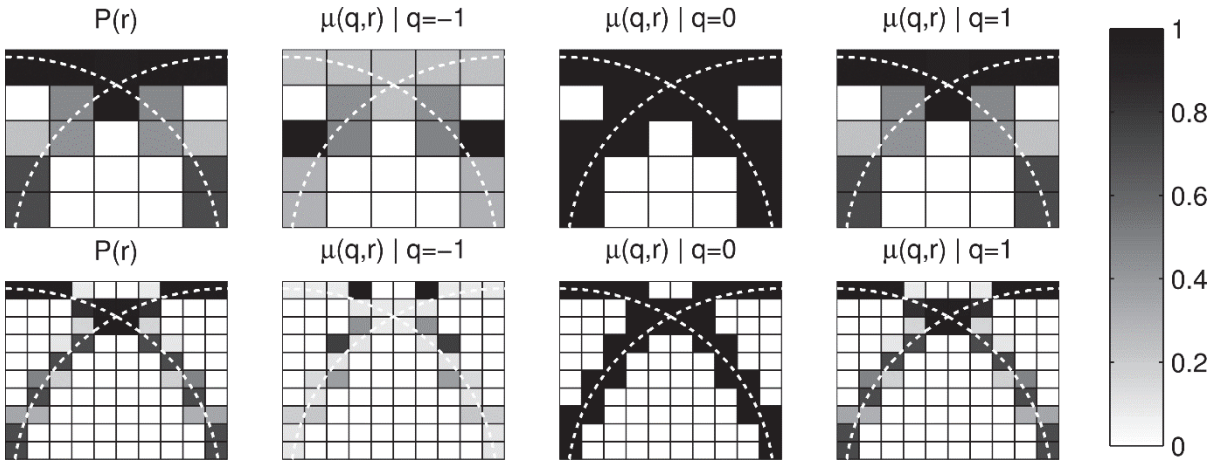

Figure 2. Probability and measure functions of synthetic cracks at q=-1, q=0, and q=1, all plots are normalized.

As it was described in section 2.1, $\alpha(q)$, $f(q)$, and D_q were calculated by using regression lines over the entire range of box sizes. Figure 3 illustrate some of these regression lines for CASE 0 (Figure 1(a)). In this figure, regression line plots for only three values of q, i.e. $q \in \{-1,0,1\}$ are shown in column wise order.

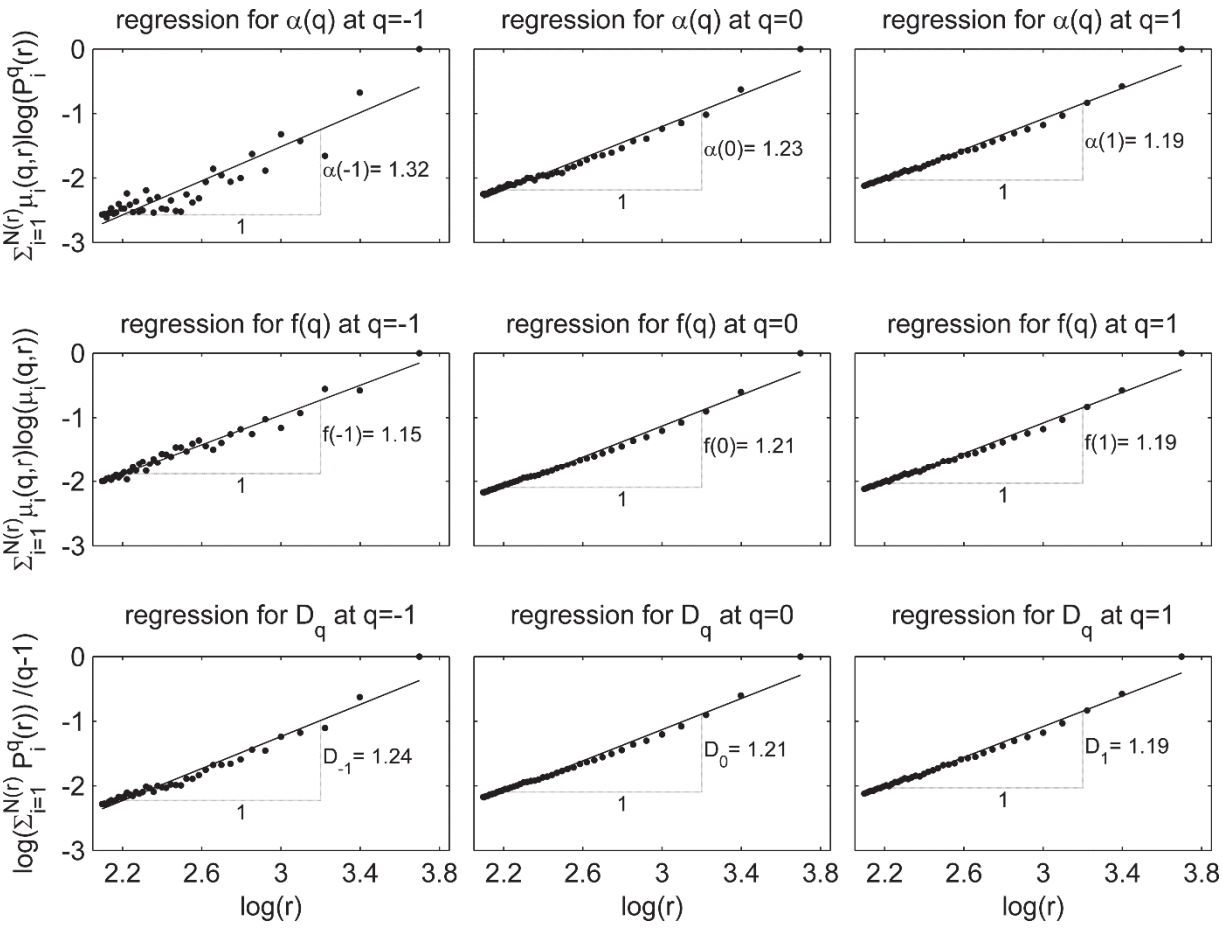

Figure 3. Regression lines on the synthetic crack pattern CASE 0's data. Note *r* is in [mm].

As illustrated in Figure 4, where $f(\alpha)$ and D_q curves are shown for the four synthetic crack patterns shown in Figure 1, multifractal analysis could provide a sensitive tool for the discrimination of crack patterns. As expected, the curves $f(\alpha)$ are convex with a single maximum at $q=0$while D_q are monotonically decreasing. The relation between α and the

parameter q, is the following: the right branch corresponds to negative values of q, the left one to positive values of q. By comparing CASE 0, and CASE 1, it can be observed that $f(\alpha)$ and D_q show negligible difference for positive values of q, whereas more significant difference can be observed for negative values of q. The reason behind this different behavior is that, q acts as a scanning tool, that is, for $q>0$ regions with high probability are amplified, while for $q<0$ regions with low probability are magnified, making the analysis more sensitive to local variations; therefore for $q>0$ the analysis focuses more on the general shape rather than local features of the input patterns. For CASE 2, since overall shape of the pattern changed, while local features were kept the same, both $f(\alpha)$ and D_q show the change just in the negative range of q. For CASE 3 it can be clearly recognized a qualitative difference in the $f(\alpha)$ and D_q curves, caused by differences in crack patterns. Therefore, it is conceivable that with the help of the multifractal analysis an automatic "early warning" of the damage progression could be implemented if the actual shape of $f(\alpha)$ and D_q curves deviates considerably from critical curves representing "normal" operating conditions.

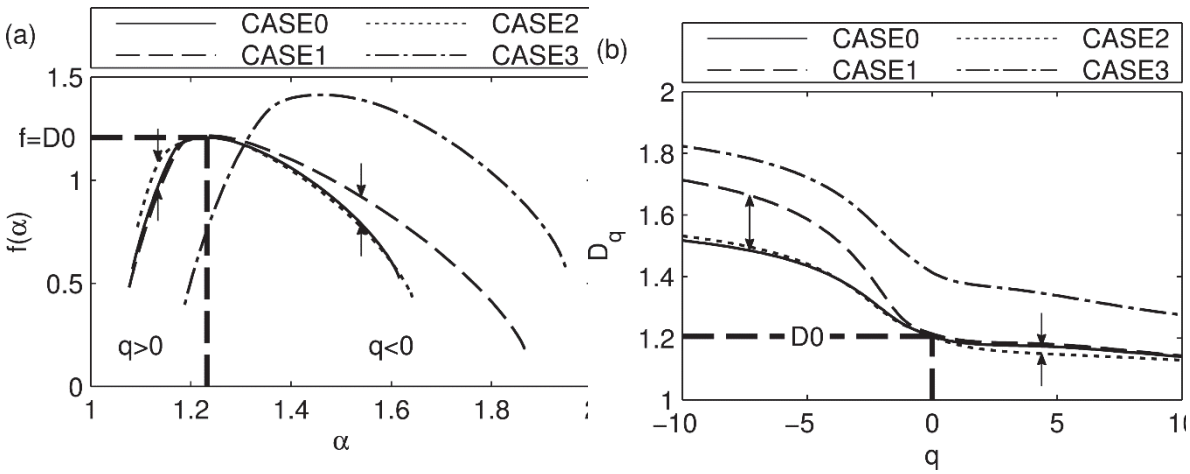

Figure 4. Singularity spectrum (a) and generalized dimension (b) of the synthetic crack patterns.

Experiments

Experimental tests were carried out on two large scale RC concrete shear walls namely SW1 and SW2 with height-to-width ratio of 0.94 and 0.54, respectively. The walls were designed in compliance with ACI 318-08 including its chapter 21, earthquake resistance structures. Figure 5 shows an overall view of the specimens, and **Table 1** summarizes their main characteristics. More details regarding specimens design can be found in the reference [36]. To simulate earthquake loading effects, each specimen was subjected to a quasi-static cyclic loading. Cyclic loads were applied by two hydraulic actuators to the top of the specimens while their foundations were fully connected to the strong floor laboratory with 14 post-tensioned, 1.5 inch nominal diameter Dywidag bars. Load transfer between the actuators and

the walls was provided with brackets and plates at sides of the wall. The plates were post-tensioned connected to each other at 450 mm bellow the top of each wall. In order to ensure synchronized loading, actuators were actively controlled with master-slave method. They were also sloped downward about 9° from horizon to prevent out-of-plane behavior. Due to typical low axial stress in low aspect ratio RCSW, axial load was not applied in these experiments.

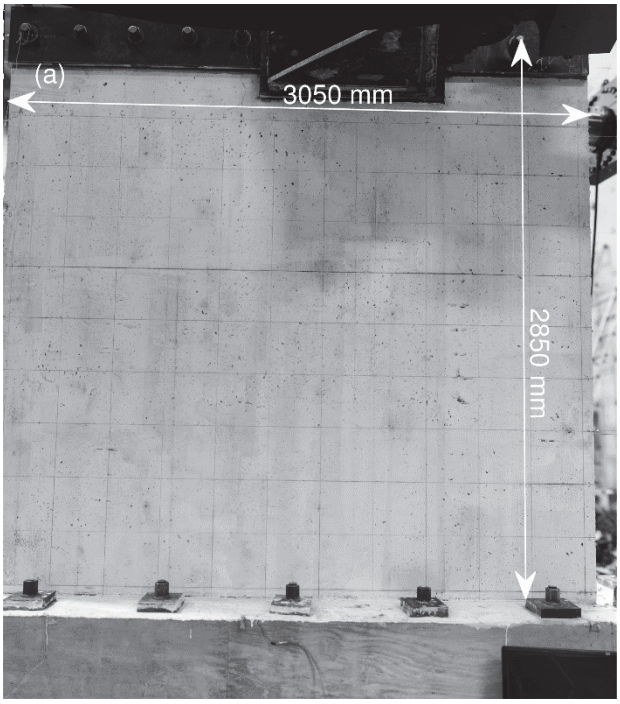

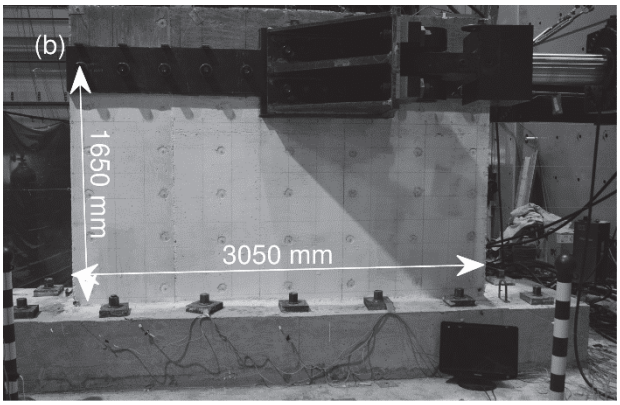

Figure 5. Experimental setup: (a) SW1, (b) SW2

Table 1. Specimens Details [37]

Characteristics	SW1	SW2
Height [mm]	3300	2100
Width [mm]	3050	3050
Thickness [mm]	200	200
Reinforcement ratio [%]	0.67	1
Wall f'_c (28^{th} day) [MPa]	21	35
Wall f'_c (test day) [MPa]	25	48.2
Rebars yield strength [MPa]	464	434
Rebars ultimate strength [MPa]	708	460

It was proposed to apply ten load steps on each wall; however, failure occurred during LS10. Each load step consisted of two load cycles, except load step zero which had there cycles. This load step was intended to verify functionality of the experimental set up and its results are not considered. Figure 6 shows the test loading protocols. Loading rate was set around 6 mm/sec and 1.3 mm/sec, respectively for SW1 and SW2. Crack mapping was carried out at each peak and zero displacement. Maximum cracks width were measured using transparent

scales, and pictures were taken at the end of each load step using a high definition camera. Due to severe crushing and spalling of SW1 at the end of experiment, and tilting of SW2 at LS10, crack monitoring was not considered at the end of the last load step.

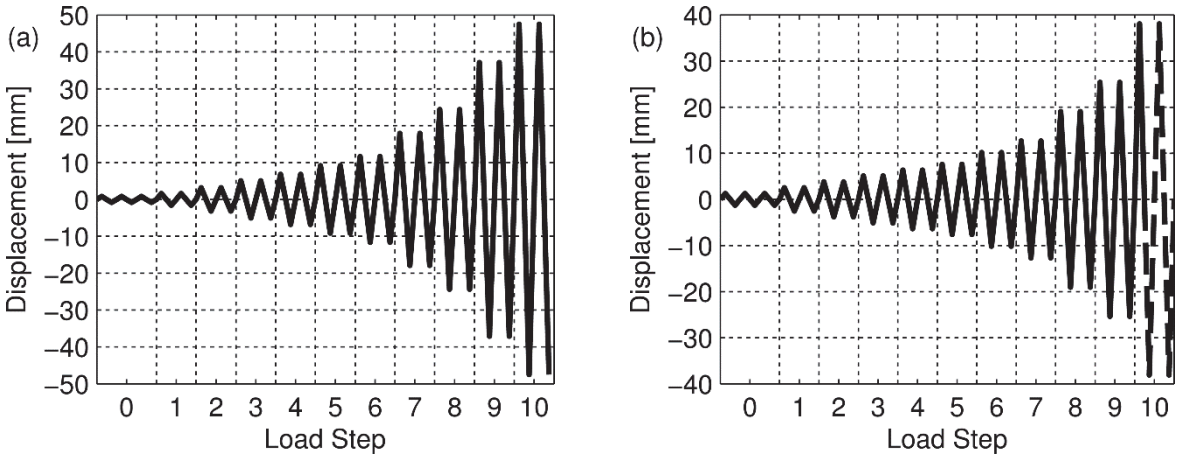

Figure 6. Load protocol [36]: (a) SW1, (b) SW2

Experimental results

Mechanical behavior

Figure 7 shows the force-displacement hysteresis loops for the two specimens. Also superimposed the trilinear backbone curve suggested by ASCE standard 41-13, for nonlinear analysis of low aspect ratio walls [38]. The trilinear backbone curves (I, II, and III) identified in Figure 7 correspond to concrete cracking (I), yielding of the reinforcement (II), and

ultimate strengths (III), observed at load steps LS2, LS6, and LS9, respectively for SW1, while at LS1, LS7 and LS9 for SW2.

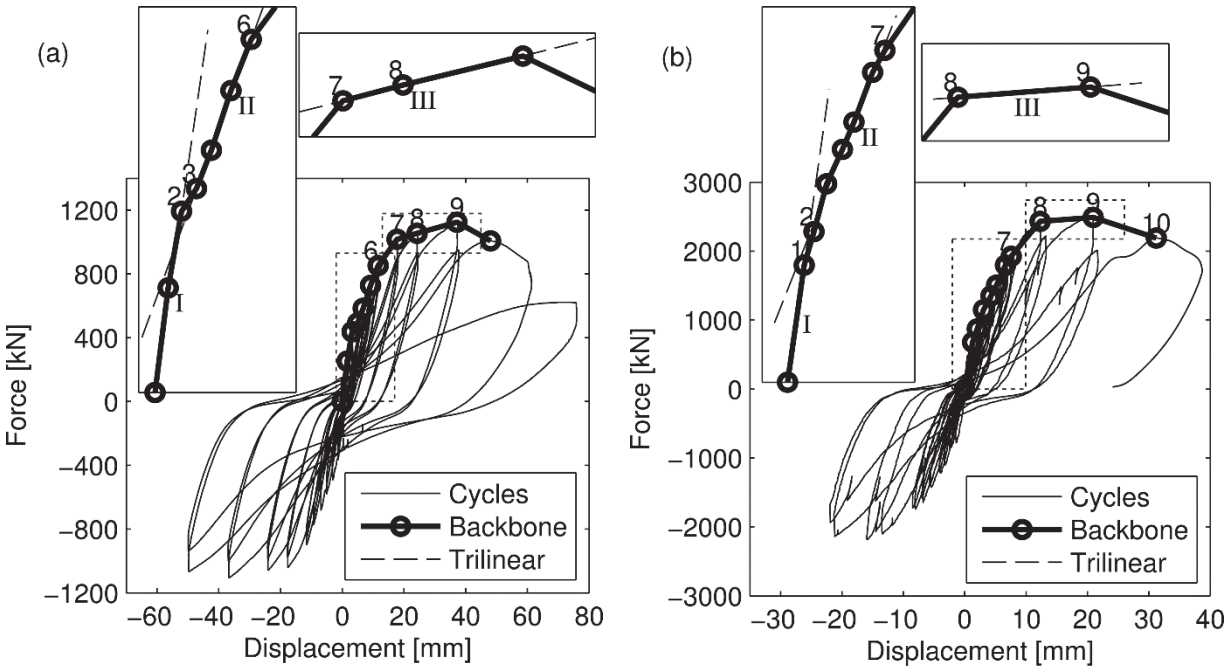

Figure 7. Force-displacement hysteresis loops [36], SW1 (a), SW2 (b)

Visual inspection

At the end of each cycle the formation of new cracks was observed while existing crack were expanded. Therefore, length or density of the cracks increased monotonically. Crack width measurements were performed at peak displacements, and zero displacements (i.e., residual cracks), for each load step. In order to categorize the severity of damage, condition-rating grades suggested by the International Atomic Energy Agency (IAEA) guidebook [5], were

adopted. Specifically, three damage grades (DG) were defined (different DG are detonated with alphabets in this paper while roman letters are used in the IAEA guidebook): grade A in which the maximum crack width was less than 0.2 mm; grade B (i.e., moderate damage) in which the largest crack width was comprised between 0.2 and 1mm; and grade C (i.e., critical damage) for cracks larger than 1mm. In general, no repair is needed for grade A, whereas appropriate rehabilitation strategy is necessary for grade B and C.

Figure 8 compares crack widths at peak and zero displacements during testing. Also superimposed the DG thresholds suggested by IAEA guidebook. For the sake of clarity, cracks at peak displacements are shown in the middle of each load steps, while residual cracks are shown at the end of each load step. It is worth noting that damage classification based on residual crack measurements may lead to underestimation of the actual severity of damage. For instance, according to the DGs assigned to SW1 based on its residual crack width, critical damage (grade C) was reached at LS8 (Figure 8(a)), while the mechanical behavior of the wall identified severe damage at LS7. Similarly, damage grade C was identified in LS9 of SW2 (Figure 8(b)), while its backbone curves show severe damage in LS8. In addition as the structure returns to its rest position, cracks close; therefore, different lateral displacements of the wall results in different crack width measurements for the same actual level of damage.

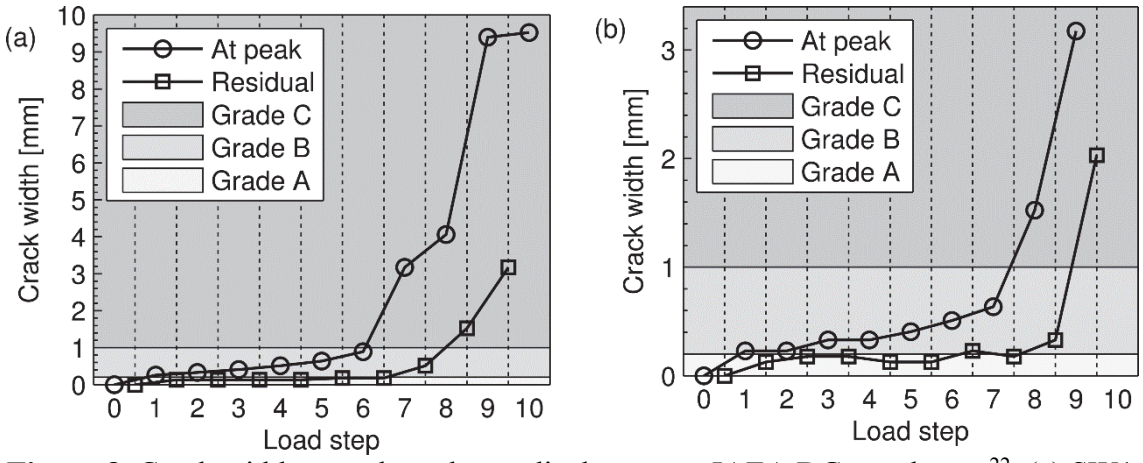

Figure 8. Crack width at peak, and zero displacement, IAEA DG are shown [22], (a) SW1, (b) SW2

Crack patterns images were also collected at the end of each load step, when the wall reached the zero displacement (residual cracks). In order to extract binary images from original ones, crack patterns were drawn manually on the original images using Adobe Photoshop, as shown in Figure 9. A complete sequence of residual crack patterns for both SW1 and SW2 can be found in [22].

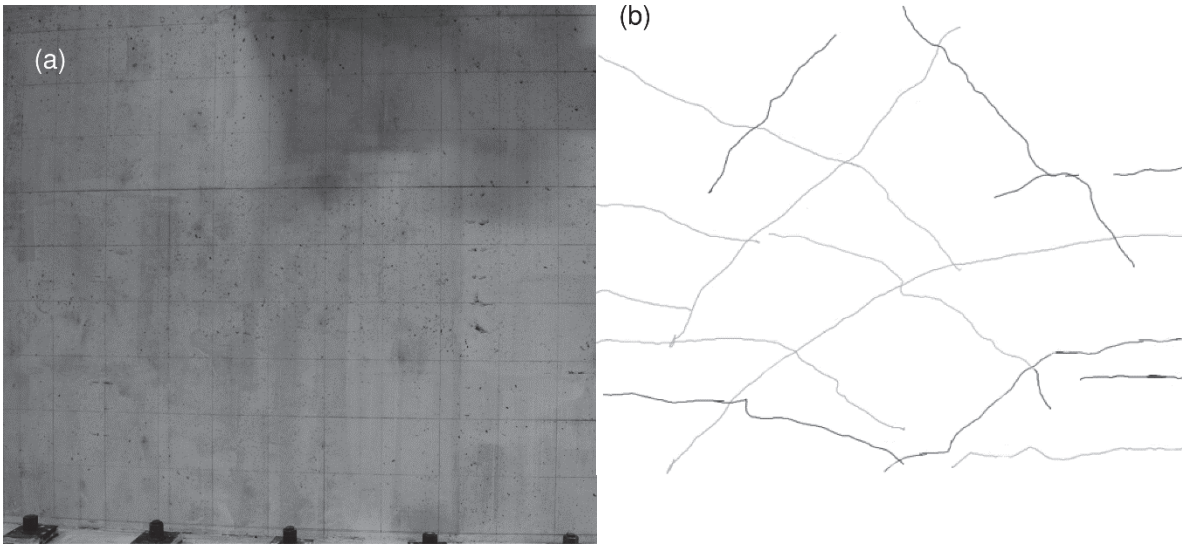

Figure 9. SW1-residual cracks after LS4: (a) original image (b) crack patterns [22]

Multifractal analysis results

The Chhabra method was used to calculate the multifractal singularity spectrum and generalized dimension for the residual cracks mapped at the end of each load step. Images were treated as binary images, composed of pixels which are either black or white. Each image was partitioned into a grid of rectangular boxes of the same width-to-length ratio of that specimen under investigation, and the box sizes ranging from the wall size to forty times smaller ones. Binary images containing crack patterns were respectively of size 552×443 and 730×322 pixels for SW1 and SW2. Therefore, the smallest boxes have short edges of at least 11 and 8 pixels respectively for SW1 and SW2.

Figure 10 illustrates $P_i(r)$ and $\mu_i(q,r)$ at scales $q \in \{-1,0,1\}$, and for two box sizes, that is, 203.3×163.2 mm, and 101.7×81.6 mm, corresponding to partitioning the original image into 15 and 30 boxes, respectively (note a portion of each wall was under the braces and not visible). As box sizes decreases, the overall area covered by the boxes decreases; as a result, the shape of the filled boxes will approach to the original shape of the crack patterns. Supposing that the mesh is large enough that all boxes are filled by at least one crack, and the entire special domain is fully covered by filled boxes. As a finer mesh covers the domain, regions having less density of cracks, are more likely to remain empty. Therefore, boxes with lower density are more likely to lose part of their area when covered by a finer mesh. These boxes are called rare events. Lower density in these boxes results in lower probability. Negative q magnifies these boxes, and eventually provides higher $\mu_i(q,r)$. On the other hand, boxes with higher density (e.g. where two cracks cross each other) are called smooth events because they are less probable to loss area as box size reduces.

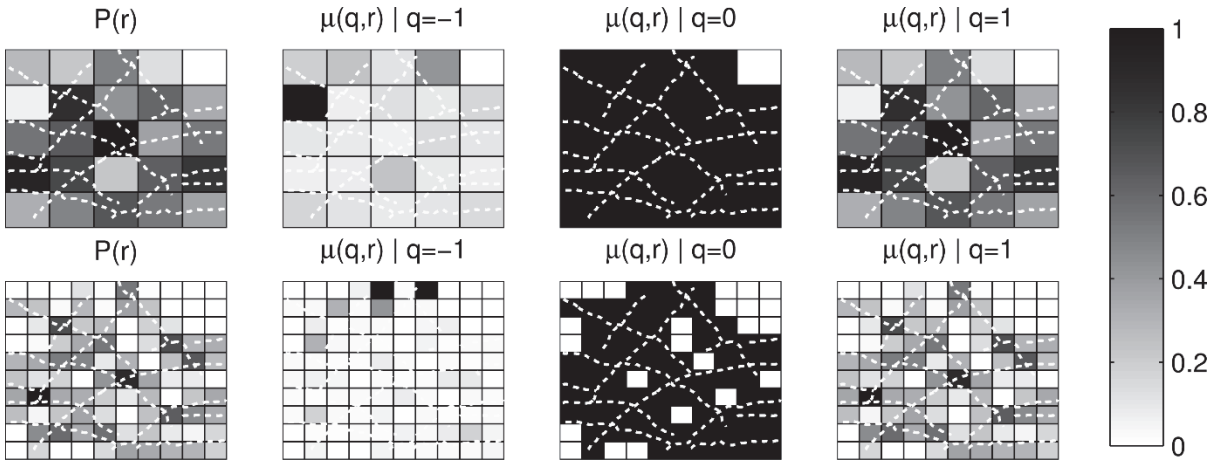

Figure 10. Probability and measure functions of SW1-LS4 cracks at different scales and box sizes

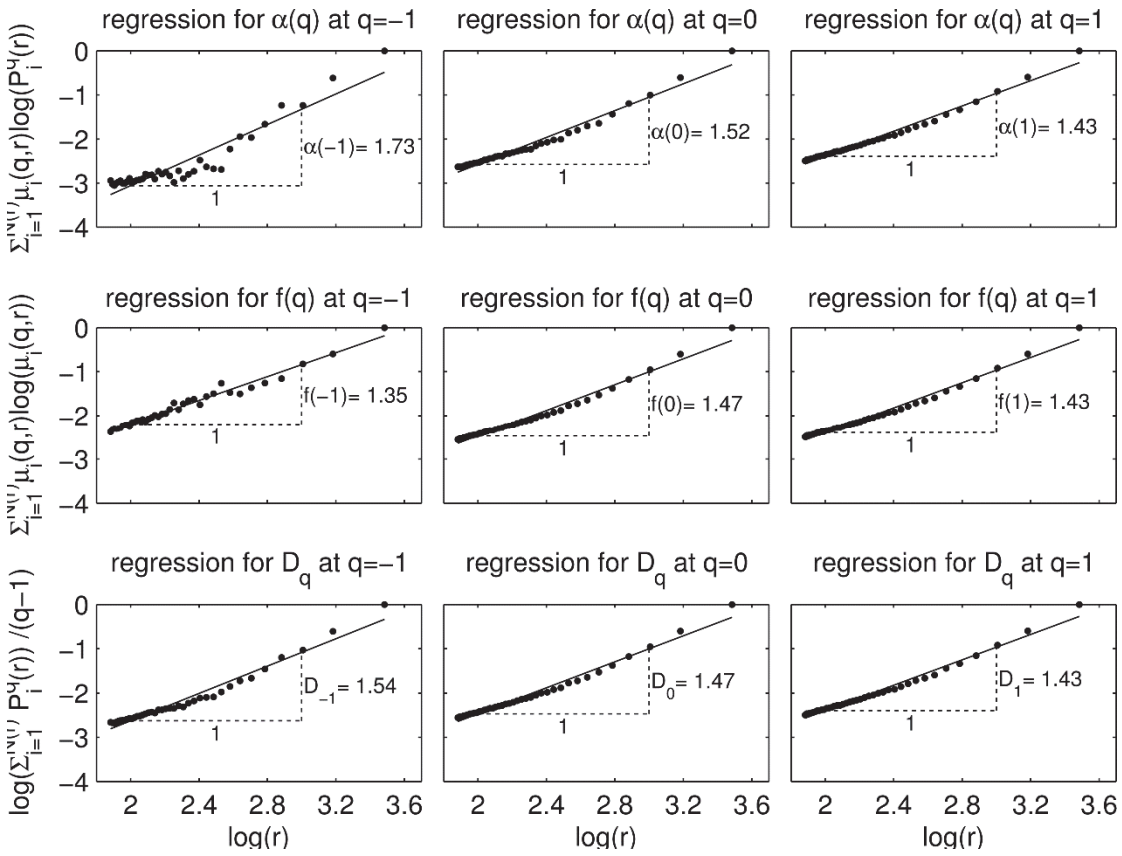

Figure 11. Regression lines for SW1-LS4 crack patterns multifractal analysis. Note r is in [mm]

Figure 11 shows regression lines fitted to data points obtained from SW1 at LS4 using different box sizes. Each columns in this figure corresponds to a different value for q, and rows correspond to regressions for different parameters. Figure 12 and Figure 13 show $f(\alpha)$

and D_q curves for SW1 and SW2 respectively. It can be seen that, as the cracks patterns extend and grow, $f(\alpha)$ and D_q curves move toward higher values, which was expected from the preliminary analysis carried out on the synthetic data (see CASE 3). Multifractal analysis tracks crack patterns changes in a spectrum of scales from local to global scales. Since cracks are monotonically increasing a monotonic increase in local scaling is expected while global changes are expected only after changes in cracking mechanism which results in generating different patterns.

In order to correlate the multifractal parameters, with the mechanical behavior of the specimens, the curves were clustered according to the trilinear backbone curve shown in Figure 7. The three clusters (I, II, III) were superimposed in Figure 13. The following observation can be made for SW1. First, significant changes for negative values of q, can be observed between load steps 2 (LS2) and 3 (LS3), where the initial yielding of the wall occurred. This may also indicate the occurrence of some minor localized cracks, similar to the CASE 1 for the synthetic data. Then, significant changes can be seen for the entire range of q (i.e., positive and negative), in the subsequent load steps in which significant yielding and stiffness degradation occurred, similar to the results predicted for CASE 3. For SW2 changes on the multifractal parameters occurred in the entire range of q, with the most

significant changes corresponding to the initial concrete cracking (I), yielding of the reinforcement (II), and ultimate strengths (III), observed at load steps at LS1, LS7 and LS9.

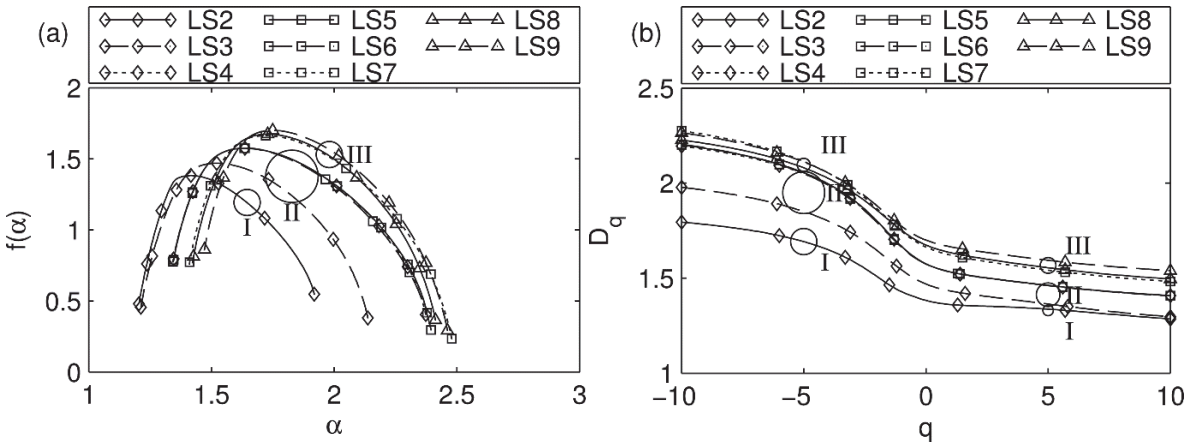

Figure 12. Multifractal analysis of SW1 at different load steps, clusters are indicated with circles and guidelines: (a) singularity spectrums, (b) generalized dimension

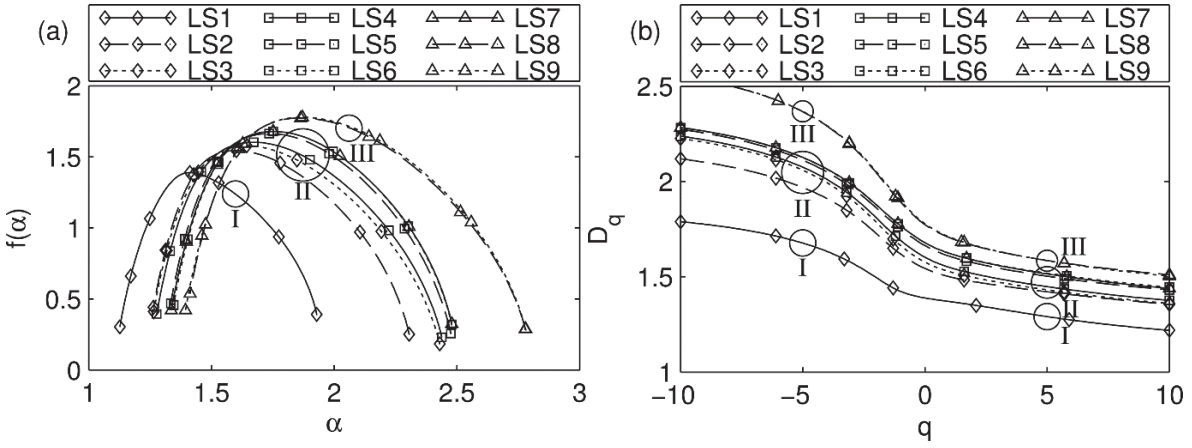

Figure 13. Multifractal analysis of SW2 at different load steps, clusters are indicated with circles and guidelines: (a) singularity spectrums, (b) generalized dimension

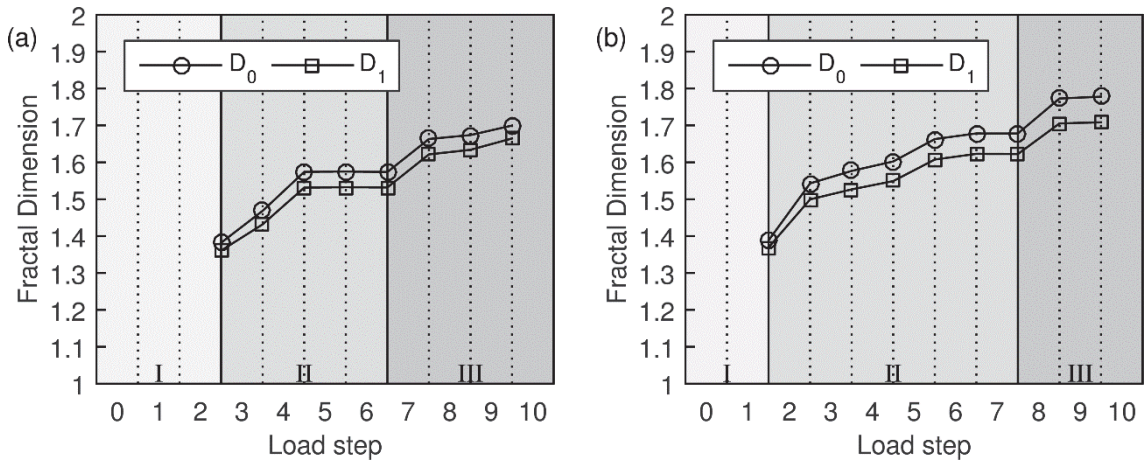

Figure 14 shows information, and correlation dimensions at various load steps, and compares them with the clusters. It can be observed that, both information and capacity dimensions of crack patterns increase monotonically with load steps, and each jump in the curve could indicate severe changes in the mechanical behavior of the structure. In addition, difference between information and capacity dimension in region I has been notably less than other regions.

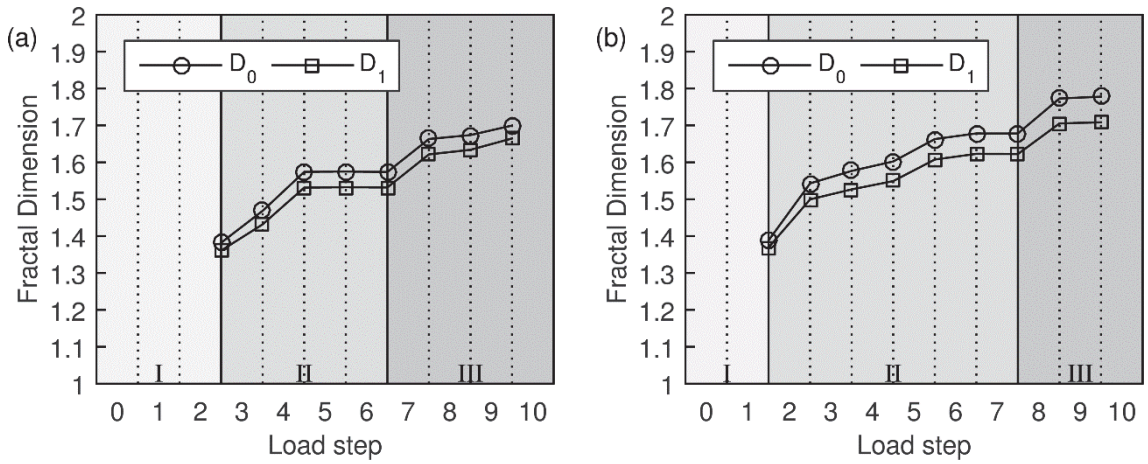

Figure 14. Capacity and information fractal dimentions at the end of each load step, multifractal clusteres are indicated with background colors: (a) SW1, (b) SW2

Conclusions

Reinforced concrete shear walls (RCSW) are one of the most commonly used seismic resisting systems in conventional buildings. Commonly, RCSWs are assessed visually by tracking defects such as corrosion and spalling, and quantifying the length and the width of existing cracks. Although manual visual inspection (VI) is a well-established method to inspect RCSWs, it is time-consuming and depends heavily on the skills of the inspectors. This paper presented an approach based on the multifractal analysis of 2D images taken in the visible spectrum, to retrieve surface defect patterns that can provide a quantitative measure of damage. Traditional multifractal parameters, including singularity spectrum and

generalized dimension curves, were first illustrated for synthetic crack patterns. Main differences between monofractal and multifractal analysis were emphasized. The approach was applied to a set of experimental data collected during testing of two large-scale RCSW subjected to controlled reversed cyclic loading in the plane of their web. In particular, the available data set included detailed records of crack images and structural performance for each test specimen. The structural response data available for each specimen was used to link the multifractal parameters with the structural performance of the two specimens. It was observed that, as the cracks patterns extend and grow, $f(\alpha)$ and D_q curves move toward higher values and jump as cracking mechanism changes. This trend was also predicted by the preliminary analysis on the synthetic crack patterns.

It is conceivable that with the help of the multifractal analysis an automatic alarming system could be implemented that will alert the appropriate engineers if the actual multifractal spectrum deviates considerably from a critical multifractal curve representing "normal" operating in a structure. However, more tests and investigations are needed to standardize the approach and define a critical multifractal curve for each RCSWs based on their specifications.

Acknowledgments

This work was supported by the National Science Foundation under Grant No. CMMI-1333506. Special thanks are also extended to Prof. Andrew Whittaker for sharing the experimental data (under Grant No. CMMI-0829978), and the technical staff at the NEES Equipment Site at the University at Buffalo.

References

1. Foudazi A, Ghasr MT, Donnell KM. Characterization of Corroded Reinforced Steel Bars by Active Microwave Thermography. *IEEE Trans Instrum Meas* 2015; PP: 1–1.

2. Farhidzadeh A, Ebrahimkhanlou A, Salamone S. Corrosion damage estimation in multi-wire steel strands using guided ultrasonic waves. In: Shull PJ (ed) *Proceedings of SPIE vol. 9437*. Anaheim, 2015, p. 94371F.

3. Schmitt TR, Darwin D. *SL Report 92-5: Bond of Epoxy-Coated Wire to Concrete*. Lawrence, 1992.

4. Lindquist WD, Darwin D, Browning JP. *SM Report 78: Cracking and Chloride Contents in Reinforced Concrete Bridge Decks*. Lawrence, 2005.

5. IAEA. *Guidebook on non-destructive testing of concrete of structures*. Vienna: International Atomic Energy Agency, 2002.

6. FHWA. *Recording and coding guide for the structure inventory and appraisal of the nation's bridges*. Washington,D.C.: Federal Highway Administration, 1995.

7. FHWA. NBIS Title 23 CFR650. In: *National Bridge Inspection Standards*. Washington,D.C.: Federal Highway Administration, 2004, pp. 74419–74439.

8. Chen Z, Hutchinson TC. Image-Based Framework for Concrete Surface Crack Monitoring and Quantification. *Adv Civ Eng* 2010; 2010: 1–18.

9. Jahanshahi MR, Masri SF. A new methodology for non-contact accurate crack width measurement through photogrammetry for automated structural safety evaluation. *Smart Mater Struct* 2013; 22: 035019.

10. Farhidzadeh A, Ebrahimkhanlou A, Salamone S. A vision-based technique for damage assessment of reinforced concrete structures. In: Kundu T (ed) *Health Monitoring of Structural and Biological Systems 2014*. San Diego, California, USA, 2014, p. 90642H.

11. Torok MM, Golparvar-Fard M, Kochersberger KB. Image-Based Automated 3D Crack Detection for Post-disaster Building Assessment. *J Comput Civ Eng* 2014; 28: A4014004.

12. Ellenberg A, Kontsos A, Bartoli I, et al. Masonry Crack Detection Application of an Unmanned Aerial Vehicle. In: *Computing in Civil and Building Engineering (2014)*. Reston, VA: American Society of Civil Engineers, 2014, pp. 1788–1795.

13. Ebrahimkhanlou A, Farhidzadeh A, Salamone S. Multifractal analysis of two-dimensional images for damage assessment of reinforced concrete structures. 2015; 9435: 94351A.

14. Lopes R, Betrouni N. Fractal and multifractal analysis: a review. *Med Image Anal* 2009; 13: 634–49.

15. Yadav RP, Dwivedi S, Mittal AK, et al. Analyzing the LiF thin films deposited at different substrate temperatures using multifractal technique. *Thin Solid Films* 2014; 562: 126–131.

16. Li L, Hu W, Liu L, et al. Evaluation of breast cancer chemotherapy efficacy with multifractal spectrum analysis of magnetic resonance image. *Biomed Mater Eng* 2014; 24: 163–71.

17. Chakraborty B, Haris K, Latha G, et al. Multifractal Approach for Seafloor Characterization. *IEEE Geosci Remote Sens Lett* 2014; 11: 54–58.

18. Sarmiento E, Uruchurtu J, Sarmiento O, et al. Fractal Analysis of the Corrosion Inhibition of Carbon Steel in a Bromide Solution by Lithium Chromate. *Electrochem Sci* 2009; 4: 144–155.

19. Moustafa A, Salamone S. Fractal dimension-based Lamb wave tomography algorithm for damage detection in plate-like structures. *J Intell Mater Syst Struct* 2012; 23: 1269–1276.

20. Bai R, Ostachowicz W, Radzie ski M, et al. Vibrational damage detection using fractal surface singularities with noncontact laser measurement. *J Vib Control* 2014.

21. Lee E-T, Eun H-C. Damage Detection of Steel Beam Using Frequency Response Function Measurement Data and Fractal Dimension. *J Vib Acoust* 2015; 137: 034503.

22. Farhidzadeh a., Dehghan-Niri E, Moustafa A, et al. Damage Assessment of Reinforced Concrete Structures Using Fractal Analysis of Residual Crack Patterns. *Exp Mech* 2013; 53: 1607–1619.

23. Ivanov PC, Amaral LA, Goldberger AL, et al. Multifractality in human heartbeat dynamics. *Nature* 1999; 399: 461–5.

24. Mandelbrot B. *The fractal geometry of nature*. New York: Henry Holt & Co, 1982.

25. Kamer Y, Ouillon G, Sornette D. Barycentric fixed-mass method for multifractal analysis. *Phys Rev E* 2013; 88: 022922.

26. Falconer K. *Fractal Geometry: Mathematical Foundations and Applications*. 3rd ed. John Wiley & Sons, 2013.

27. Reljin I, Reljin B. Fractal geometry and multifractals in analyzing and processing medical data and images. *Arch Oncol* 2002; 10: 283–293.

28. Theiler J. Estimating fractal dimension. *J Opt Soc Am A* 1990; 7: 1055.

29. Voss RF. Voss, R.F. 1988. Fractals in nature: From characterization to simulation. In: *The Science of Fractal Images*. New York: Springer New York, 1988, p. pp 21–70.

30. Weiss J. Fracture and fragmentation of ice: a fractal analysis of scale invariance. *Eng Fract Mech* 2001; 68: 1975–2012.

31. Harte D. *Multifractals: Theory and Applications*. London.: CRC Press, 2001.

32. Rényi A. On measures of information and entropy. In: *Proceedings of the fourth Berkeley Symposium on Mathematics, Statistics and Probability*. Berkeley: University of California Press, 1961, pp. 547–561.

33. Cao M, Ren Q, Qiao P. Nondestructive Assessment of Reinforced Concrete Structures Based on Fractal Damage Characteristic Factors. *J Eng Mech* 2006; 132: 924–931.

34. Chhabra A, Jensen R. Direct determination of the f(α) singularity spectrum. *Phys Rev Lett* 1989; 62: 1327–1330.

35. Chhabra A, Meneveau C, Jensen R, et al. Direct determination of the f(α) singularity spectrum and its application to fully developed turbulence. *Phys Rev A* 1989; 40: 5284–5294.

36. Rocks JF. *Large Scale Testing of Low Aspect Ratio Reinforced Concrete Walls.* the State University of New York at Buffalo, 2012.

37. Luna B, Rivera J, Rocks J, et al. University at Buffalo - Low Aspect Ratio Rectangular Reinforced Concrete Shear Wall - Specimen SW1. 2013.

38. ASCE/SEI. *Asce Standard 41-13 Seismic Evaluation and Retrofit of Existing Buildings*. 2013th ed. Reston: American Society of Civil Engineers, 2014.